AGU PUBLICATIONS

JGR

Journal of Geophysical Research: Atmospheres

RESEARCH ARTICLE
10.1002/2016JD024768

Key Points:
- Growing cumulus clouds were analyzed toward predicting early severe weather
- Temperature–effective radius and convective initiation fields delineated storm intensity
- Multivariate analysis was used to for a simple predictive model for storm severity

Correspondence to:
J. R. Mecikalski,
johnm@nsstc.uah.edu

Citation:
Mecikalski, J. R., D. Rosenfeld, and A. Manzato (2016), Evaluation of geostationary satellite observations and the development of a 1–2 h prediction model for future storm intensity, *J. Geophys. Res. Atmos.*, *121*, 6374–6392, doi:10.1002/2016JD024768.

Received 6 JAN 2016
Accepted 13 MAY 2016
Accepted article online 16 MAY 2016
Published online 9 JUN 2016

Evaluation of geostationary satellite observations and the development of a 1–2 h prediction model for future storm intensity

John R. Mecikalski[1], Daniel Rosenfeld[2], and Agostino Manzato[3]

[1]Atmospheric Science Department, University of Alabama in Huntsville, Huntsville, Alabama, USA, [2]Institute of Earth Sciences, The Hebrew University, Jerusalem, Israel, [3]OSMER (Osservatorio Meteorologico Regionale), dell'ARPA Friuli Venezia Giulia, Visco (UD), Italy

Abstract A study was conducted to gain insights into the use of geostationary satellite-based indicators for characterizing and identifying growing cumulus clouds that evolve into severe weather producing convective storms. Eleven convective initiation (CI), 41 cloud top temperature–effective radius (T-r_e), and 9 additional fields were formed for 340 growing cumulus clouds that were manually tracked for 2 h and checked for association with severe weather to 2–3 h into the future. The geostationary satellite data were at 5 min resolution from *Meteosat-8* on six convectively active days in 2010, 2012, and 2013. The study's goals were to determine which satellite fields are useful to forecasting severe storms and to form a simple model for predicting future storm intensity. The CI fields were applied on 3×3 pixel regions, and the T-r_e fields were analyzed on 9×9 and 51×51 pixel domains (needed when forming T-r_e vertical profiles). Of the 340 growing cumulus clouds examined, 34 were later associated with severe weather (using European Severe Weather Database reports), with the remaining being nonsevere storms. Using a multivariate analysis, transforming predictors into their empirical posterior probability, and maximizing the Peirce skill score, the best predictors were T_{1451} (51×51 pixel T, where r_e exceeds 14 μm), T_{G9} (9×9 pixel glaciation T surrounding a growing cloud), and Re_{BRTG51} (51×51 pixel r_e at the breakpoint T in the T-r_e profile). Rapid cloud growth prior to severe storm formation leads to delayed particle growth, colder temperatures of the first 14 μm particles, and lower T_G values.

1. Introduction

As outlined in *Mecikalski et al.* [2015], a significant amount of effort has been spent on obtaining highly accurate short-term forecasts of the initiation of convective storms in light of the high impact that poor thunderstorm forecasts have on various activities (e.g., air travel) and public safety. An ideal platform for providing an early warning capability for the initiation of convective storms is the 5–15 min resolution of geostationary satellite observations [*Purdom*, 1976, 1982; *Roberts and Rutledge*, 2003; *Mecikalski and Bedka*, 2006; *Rosenfeld et al.*, 2008a; *Mecikalski et al.*, 2010a, 2010b, 2015]. The Geostationary Operational Environmental Satellite (GOES), *Feng-Yun*, Multifunctional Transport SATellite, *Meteosat*, and *Himawari* offer near-global 55°N to 55°S coverage with 500 m to 4 km spatial resolution in visible and near-infrared channels and at 2–4 km in infrared (IR) channels. A number of methods and algorithms exist to process these satellite data in real time to monitor convective clouds [*Merk and Zinner*, 2013], convective storm initiation (CI) in the 0–1 h time frame [*Roberts and Rutledge*, 2003; *Mecikalski and Bedka*, 2006; *Mecikalski et al.*, 2010a, 2010b, 2015; *Walker et al.*, 2012; *Nisi et al.*, 2014], or severe storm initiation [*Lensky and Rosenfeld*, 2006; *Rosenfeld et al.*, 2008a; *Cintineo et al.*, 2014]. The accuracies of CI prediction methods are in the 70–85% range or slightly higher depending on the environment [*Mecikalski et al.*, 2015].

Emphasis needs to be placed on extending the CI nowcasting algorithms by integrating satellite, radar, numerical weather prediction (NWP) models, and other data sets (e.g., lightning) to provide forecasts with increased lead time to high-impact events such as severe storms. *Fritsch et al.* [1998], *Curran et al.* [2000], *Evans and Ducot* [2006], and *Wolfson and Clark* [2006] have quantified the impacts that strong thunderstorms have on travel, air traffic, infrastructure, and society. *Changnon* [2001], *Brooks et al.* [2003], *Brooks and Dotzek* [2007], *Dixon et al.* [2011], and others have identified the costs of convective weather in terms of storm-related hazards (hail, high winds, flooding, and tornadoes), which motivates the need for more precise early detection methods for severe thunderstorms, using all available observational data sets. Along these lines, *Hartung et al.* [2013] examined how GOES 10.7 μm channel cloud top cooling rates correlate with later time rainfall intensity and large hail. *Cintineo et al.* [2013] determined the distributions of GOES satellite-retrieved

cloud properties in severe and nonsevere storms, while *Cintineo et al*. [2014] combined GOES cloud properties, radar, and NWP fields to forecast severe storm potential. These studies using GOES imagery have shown that severe storms can develop very rapidly, from small cumulus clouds to a cumulonimbus producing heavy rainfall, damaging wind, hail, and/or a tornado occurring in as little as 1 h [*Cintineo et al*., 2013]. Similarly, rapid cumulus cloud top cooling during CI is correlated with severe weather [*Hartung et al*., 2013; *Cintineo et al*., 2013]. *Lensky and Rosenfeld* [2006] and *Rosenfeld et al*. [2008b] have demonstrated that key cloud top microphysical signatures coupled with rapid cloud development provide substantial indication of severe weather occurrence.

The methods by *Rosenfeld et al*. [2006, 2008a] and *Lensky and Rosenfeld* [2006] have demonstrated a correlation between the temperature of a cumulus cloud's top (T_{TOP}) and particle effective radius (r_e), as functions of aerosol contents and updraft strength, developing T_{TOP} versus r_e diagrams as a function of altitude. The T_{TOP}-r_e [or $T(z)$-$r_e(z)$, "T-r_e"] diagrams are formed using an ensemble of clouds in various stages of development across the region. In these studies, it was proposed that *relative* updraft strength (with respect to surrounding updrafts), and hence the vigor of the new convective storms, can be estimated from cloud top r_e values, and hence, one can predict storm intensity using T-r_e metrics. In this study, we assume that the aerosol distribution (or cloud concentration nuclei) is generally similar across a meso-β scale (25–250 km) region analyzed for severe storm development within a 1–2 h time frame. These metrics include the glaciation temperature (T_G), the r_e at T_G, and other parameters that quantify the profile of T_G versus r_e (as listed in Table 1). Figure 1 shows T-r_e diagrams as a function of updraft intensity. Although CI algorithms [*Mecikalski et al*., 2015] provide predictions of convective rainfall of ≥35 dBZ intensity, until now they do not provide estimates of which CI events will lead to severe convective storms. Included with the CI interest fields as described in previous studies [*Mecikalski and Bedka*, 2006; *Mecikalski et al*., 2010a, 2010b] are satellite-retrieved cloud parameters, such as r_e, optical depth, and indicators of cloud top phase, which have been shown to add skill to the CI nowcasts by improving understanding of the physical processes important to the CI processes, such as increasing cloud depth over time, updraft integrity (width and depth), and glaciation related to precipitation production [*Mecikalski et al*., 2011].

Soundings of moisture and especially wind shear from NWP models complement satellite-observed cloud top temperature information and inferred in-cloud dynamics by helping to identify favorable environmental conditions for the formation of severe convection. *Cintineo et al*. [2013] and *Mecikalski et al*. [2015] have recently shown how Bayesian probability methods, and machine learning (logistic regression [*Hosmer and Lemeshow*, 1989] and random forest [*Pal*, 2005; *Diaz-Uriarte and de Alvarez*, 2006; *Williams et al*., 2008; *Williams*, 2014]), respectively, can be applied to convective storm nowcasting, which emphasizes the value in combining information from various sources. Similarly, within the AutoNowcaster, a combination of interest field thresholds and fuzzy logic membership functions from several input data sources generate combined likelihood fields that are integrated into CI nowcast zones [*Mueller et al*., 1993, 2003].

The goal of this study is to evaluate hitherto two *Meteosat-8* satellite-based methods in a combined fashion for predicting the initiation [e.g., *Mecikalski and Bedka*, 2006; *Mecikalski et al*., 2010a] and the near-term intensity of convective storms [*Rosenfeld et al*., 2008a], forming then a subset of predictors and a simple model that can be used to predict in advance the initiation of locally intense or severe convective storms, as classified by the European Severe Weather Database (ESWD; http://www.eswd.eu) [*Dotzek et al*., 2009]. This study then represents one of the first attempts to apply such a methodology over the European territory.

Sixty-one candidate predictor variables (Table 1) are developed from 5 min resolution *Meteosat-8* Spinning Enhanced Visible and Infrared Imager (SEVIRI) observations over the 0–45 min time frame of cumulus cloud development. These cumulus cloud-focused parameters are analyzed on a per-storm basis and compared to mature storm behavior and severe weather reports 2–3 h into the future. In the end, a much reduced list of predictors is developed, followed by procedures for applying them in a simple prediction system. The study's outcome demonstrates the value of satellite observations in a manner that extends nowcasting (0–3 h short-term forecasts) for forecasters of severe convective storms.

The paper proceeds as follows: section 2 provides a more in-depth background on the CI and T-r_e algorithms, while section 3 describes the main data sets used in the study and also outlines the project methodology and analysis techniques employed herein. Section 4 shows the results, and section 5 discusses the main findings and concludes the paper.

Table 1. The List of All 61 Predictor Variables That Were Collected for This Study[a]

Interest Field	Description
Date	YYYYMMDD
Storm	Number of tracked storm
Map	Frame number in the storm tracking (1 to 25, for 0 to 2 h every 5 min)
Hour	Decimal hour
Latitude	Latitude of the center of the matrix (decimal degrees)
Longitude	Longitude of the center of the matrix (decimal degrees)
i_{CENTER}	*I* coordinate of the center of the flagged storm
j_{CENTER}	*J* coordinate of the center of the flagged storm
Radius	Equivalent circle radius of the cell in number of pixels
	***T*-r_e fields: (storm—9 × 9 pixels) and (environment—51 × 51 pixels) arithmetic average**
T_{TOP}	Storm and environment lowest top temperature (°C)
T_G	Storm and environment glaciation temperature (°C)
T_{BRTG}	Storm and environment *T* of breakpoint of the *T*-r_e line (°C)
T_{14}	Storm and environment *T* where r_e exceeds 14 μm (°C)
T_B	Storm and environment *T* of cloud base or warmest cloudy pixel (°C)
dSLOPE*10	Storm and environment slope of lower part minus slope of upper part of the *T*-r_e line (μm/°C)
Re_{TOP}	Storm and environment r_e at T_{TOP51} (μm)
Re_{GLAC}	Storm and environment r_e at T_{G51} (μm)
Re_{BRTG}	Storm and environment r_e at T_{BRTG51} (μm)
Exp/10	Storm and environment expansion rate of the cloud top, as defined by the coldest 10 *T*°C (pixel2/5 min)
fExp*10	Storm and environment fractional expansion rate, defined by Exp9 cloud top area (unitless)
COR_{TBTG}	Storm and environment correlation of the *T*-r_e points (unitless)
***S* (cumulative)**	Storm and environment—cumulative score environment: $S_{dSLOPE51} + S_{TG51} + S_{TBR51} + S_{REG51} + S_{REBR51}$
S (multiply)	Storm and environment—multiplied score environment: $S_{dSLOPE51} \times S_{TG51} \times S_{TBR51} \times S_{REG51} \times S_{REB51}$
S_{dSLOPE}	Storm and environment—break in the slope in μm/°C. Smaller > linear and more severe. dSlope51 × 10 = 0 > 1; 5 > 0
S_{TG}	Storm and environment—colder T_{G51} indicates more severe storm. $T_{G51} = -40°C > 1$; −25 > 0
S_{TBR}	Storm and environment—colder temperature of the breakpoint below T_{G51} is more severe. $T_{BRTG51} = -38C > 1$; −23 > 0
S_{REG}	Storm and environment—smaller Re_{GLAC51} is more severe. Re_{GLAC51} <20 μm > 1; 40 μm > 0.25
S_{REBR}	Storm and environment—smaller Re_{BR51} is more severe. Re_{BRTG51} <20 μm > 1; 40 μm > 0.25
***S* (fExp51)**	Region—larger cloud top fractional expansion is more severe. fExp51 × 10 = 0.333 > 1; 0 > 0
***S* (overshoot51)**	Region—deeper overshoot is more severe. 6.2–7.3 μm = 2 > 1; 0 > 0
$COOLING_9$	Cell (9 × 9) cooling rate (°C/5 min)
	Convective initiation fields: cloud scale (3 × 3 pixels) coldest pixel
6.2–7.3 μm T_B	3 × 3 pixel brightness temperature difference of 6.2–7.3 μm (°C)
8.7–10.8 μm T_B	3 × 3 pixel brightness temperature difference of 8.7–10.8 μm (°C)
3.9 μm reflectance	3 × 3 pixel 3.9 μm reflectance (unitless)
Tri-Spectral T_B	3 × 3 pixel brightness temperature difference of [(8.7–10.8 μm) − (10.8–12.0)] (μm)
12–10.8 μm T_B	3 × 3 pixel brightness temperature difference of 8.7–10.8 μm (°C)
5 min 10.8 μm trend	3 × 3 pixel 5 min 10.8 μm cloud top cooling rate (°C/5 min)
5 min 6.2–10.8 μm trend	3 ×3 pixel 5 min 6.2–10.8 μm channel difference trend (°C/5 min)
5 min 8.7–10.8 μm trend	3 × 3 pixel 5 min 8.7–10.8 μm channel difference trend (°C/5 min)
5 min Tri-Spectral trend	3 × 3 pixel 5 min trispectral channel difference trend (°C/5 min)
5 min 6.2–7.3 μm trend	3 × 3 pixel 5 min 6.2–7.3 μm channel difference trend (°C/5 min)
5 min 3.9–10.8 μm trend	3 × 3 pixel 5 min 3.9–10.8 μm channel difference trend (°C/5 min)

[a]The 47 fields that were analyzed for this study are highlighted in **bold**. Field definitions and descriptions are provided.

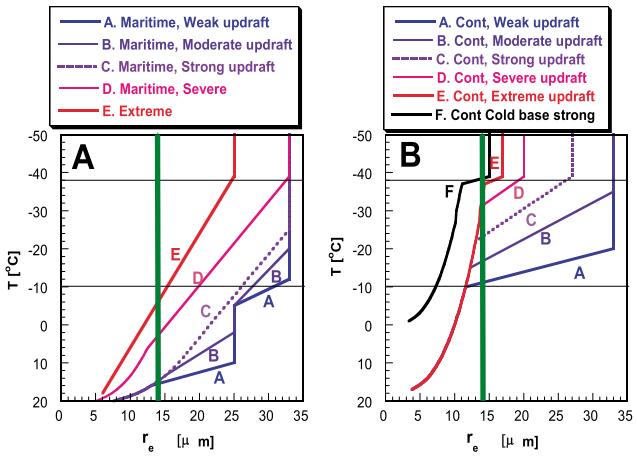

Figure 1. A conceptual model adapted from *Rosenfeld et al.* [2008a] of the way T-r_e relations of convective clouds are affected by enhanced updrafts to extreme values. The vertical green line represents the precipitation threshold of $r_e = 14\ \mu m$ [*Rosenfeld and Gutman*, 1994]. The horizontal line at $T = -38°C$ represents the homogeneous freezing isotherm. (a) Microphysically maritime clouds with low and warm bases and small concentrations of cloud concentration nuclei (CCNs) and (b) continental clouds with high CCN concentrations or high and cold bases. In reality most cases occur between these two end types.

2. Satellite Analyses of Growing Cumulus Clouds

The main hypothesis guiding this study is that time series observed only from geostationary satellite cloud top information of early stage growing cumulus clouds can be used to identify forthcoming severe weather. Therefore, in the CI and T-r_e fields, there should be a clear delineation between growing convective clouds that later produce severe weather, as compared to those clouds that do not. Furthermore, use of a small number of CI and T-r_e fields should be valuable within a statistical model that identifies forthcoming severe weather events.

2.1. Convective Initiation Nowcasting

The study by *Mecikalski and Bedka* [2006] outlined the concepts of the *GOES-R* CI algorithm, with further refinements described in *Harris et al.* [2010], *Mecikalski et al.* [2010a, 2010b], *Walker et al.* [2012], and *Mecikalski et al.* [2015]. *GOES-R* CI identifies precursor signals of CI of cumulus clouds within sequences of 500 m to 1 km resolution visible and 2–4 km IR imagery from *Meteosat*, GOES, or the forthcoming GOES-R era instruments and measures three physical components of growing convective clouds toward making a nowcast of CI valid over a 1 h period: cloud depth, cloud growth rate, and cloud top glaciation. CI is defined as the first detection of reflectivity ≥35 dBZ (a radar identified convective rainfall rate) at the −10°C level in convective clouds [*Browning and Atlas*, 1965; *Wilson and Schreiber*, 1986; *Wilson et al.*, 1992; *Wilson and Mueller*, 1993; *Mueller et al.*, 2003]. CI nowcasts are made possible by the coincident use of three components of GOES and *Meteosat* data: (1) a cumulus cloud mask at 1 km resolution [*Berendes et al.*, 2008], (2) satellite-derived mesoscale atmospheric motion vectors for tracking individual cumulus clouds [*Bedka and Mecikalski*, 2005; *Bedka et al.*, 2009], and (3) IR brightness temperature (T_B) and multispectral band differencing time trends. Despite the central wavelengths of channels differing between GOES and *Meteosat*, the main attributes measured by these instruments as listed above will be captured, with the exception that *Meteosat* affords a more robust method for measuring cloud top glaciation given the presence of the 8.5 μm channel [*Mecikalski et al.*, 2010a]. By 2012 the *GOES-R* CI algorithm routinely used 15 National Oceanic and Atmospheric Administration (NOAA) Rapid Update model and 10 GOES satellite fields in a logistic regression model, forming a 0–100% probability of CI per each convective cloud object [*Walker et al.*, 2012; *Mecikalski et al.*, 2015], and is therefore a day-night multisensor approach. Presently, the algorithm uses Algorithm Working Group Cloud Height Algorithm satellite-derived cloud parameters [*Heidinger and Pavolonis*, 2009; *Walther et al.*, 2011; *Walther and Heidinger*, 2012] to detect CI beneath cirrus [*Mecikalski et al.*, 2013] and enhance the nighttime detection of growing cumulus clouds [*Mecikalski et al.*, 2011].

The present study is along the lines of *Cintineo et al.* [2014], however focused entirely on satellite observations from European Organisation for the Exploitation of Meteorological Satellites (EUMETSAT) *Meteosat-8* when attempting to delineate percussive signatures for severe and nonsevere events. Unlike *Cintineo et al.* [2013, 2014], the present study exploits the T-r_e methodology, as originally developed and used to help identify severe weather occurrence by *Rosenfeld et al.* [2008b]. As noted, one main goal then is to provide an assessment of combined CI and T-r_e field characteristics for known weak to severe convective storms, which then may be used within CI nowcast systems, especially in light of what *GOES-R* will soon offer (as similar to *Meteosat-8*). This present study draws together satellite-based CI and a number of T-r_e fields in a manner not done previously.

2.2. T-r_e Framework

Rosenfeld et al. [2008a] provided the scientific basis and background for a conceptual model that facilitates the detection of the vigor of convective clouds and storms by remote sensing from satellites, based on the retrieved vertical profiles of cloud-particle r_e and thermodynamic phase. High updraft speeds in convective clouds, formed in conditions of high convective available potential energy (CAPE; $\geq$3000 J kg^{-1}), help sustain the presence and growth of large hailstones. Wind shear provides additional energy for organizing and sustaining supercell storms and squall lines, well known to produce damaging winds and recirculate large hail or produce widespread strong downdrafts, downbursts, and intense gust fronts. The respective roles of CAPE and 0–6 km vertical wind shear have long been known as the main predictors for severe convective storms [*Rasmussen and Blanchard*, 1998; *Hamill and Church*, 2000; *Brooks et al*., 2003].

Cloud particles have been observed to remain smaller and freeze at colder temperatures in stronger updrafts, constituting a *satellite-based severe storm microphysical signature* [*Rosenfeld et al*., 2006], with a conceptual example shown in Figure 1, as adapted from *Rosenfeld et al*. [2008a] and as validated by aircraft measurements [e.g., *Rosenfeld and Woodley*, 2000]. Use of severe storm microphysical signatures, as retrieved from 15 min resolution imagery of *GOES–11/–13*, has already shown considerable predictive skill for cloud clusters that are prone to develop into severe storms. Key cloud top microphysical features have been observed for convective clouds, often well before the initial development of an organized storm, with a forecast lead time of up to 2 h to the actual occurrence of severe weather when tested operationally at the NOAA Storm Prediction Center (SPC) [*Rosenfeld et al*., 2008b]. It is important to note that application of "water-only r_e" to predict the probability of specific clouds to become severe (as done in *Cintineo et al*. [2013], instead of applying r_e of both water and ice to the prestorm cloud cluster, misses most of the long lead-time predictive skill.

In *Rosenfeld et al*. [2008b], a method was developed to provide satellite, microphysically based, "early alerts" (EAs) of severe convective storms. The objective was to predict when and where severe weather is most likely to occur 1–2 h prior to the actual event. As such, an EA came after a Severe Weather Watch was issued by the SPC and before a National Weather Service Forecast Office issued a warning when the event is under way. An evaluation of the EA method was done at the SPC in April, May, and early June 2008. *GOES–11 and –12* multispectral imagery data were used, with the focus on severe storms. The results showed that the EA method was successful in flagging imminent severe weather events on a scale of 100 × 100 km (10^4 km^2), which was an average of 1–2 h before they occurred. It was found that the EA methodology provided valuable supporting evidence that severe weather was imminent from a growing convective cloud and therefore was useful in the SPC forecasting environment [*Rosenfeld et al*., 2008b]. This suggests that the T-r_e-based EA methodology is a potentially valuable tool for those tasked with issuing watches and warnings for severe convective storms. Unlike the SPC demonstration, the present study evaluated the potential value that T-r_e fields have in nowcasting severe storms using *Meteosat* observations, at a similar 5 min time frequency as done for the CI fields.

3. Data and Processing Methodology

Table 2 lists the "growing cumulus cloud storm" data that were collected over Europe and comprise the main data set in this study. A total of 6 days were selected, with 340 convective storms cataloged, each one having 25 time frames (25 × 5 min = 2 h). Each 5 min time will be referred to here as a "case." Table 2 also lists the number of growing cumulus cloud/storm events that were cataloged, along with the number of "severe" storms on a given day or one associated with ESWD-observed severe weather. Only "QC2" quality reports (defined as "severe event fully verified") from the ESWD were used in this study. Table 2 also lists the general region in Europe where the storms occurred. Figures 2a–2f show an example of nonsevere (09:44–10:14 UTC 15 August 2010; Figures 2a–2c) and severe (12:59–13:29 UTC 29 July 2013; Figures 2d–2f) storms in 15 min resolution *Meteosat* observations. Related to the two storms shown in Figures 2a–2f, Figures 3a and 3b present the 5 min trends in five T-r_e and the Tri-Spectral fields (see Table 1) over the first 30 min of cumulus cloud development. The clear differences seen between the growing cumulus clouds for the eventual "weak" and severe storms include (1) much warmer glaciation temperatures (T_{G9}) from 0 to 25 min for the weak storm, indicating the lack of a rapidly developing cumulus cloud; much colder T_{G9} temperatures are seen for the severe storm; (2) colder T_{1451} temperatures (by 3–5°C) for the severe versus weak storm; (3) larger particle effective radius values at the temperature of the breakpoint of the T-r_e line (Table 1) in the severe storms

Table 2. List of Severe Weather Days Analyzed[a]

Date	Cases	Severe Events	Location
15 August 2010	143	7	Western and central Europe
1 July 2012	26	2	Western and central Europe
7 July 2012	50	7	Western and central Europe
21 July 2012	27	4	Western and central Europe
20 June 2013	62	12	Central Europe
29 July 2013	32	5	Central Europe
Totals	340	34	

[a]A total of 340 growing convective cloud/storm events were analyzed. The rough regions in Europe are listed for each day. The number of severe events is listed as determined from reports in the European Severe Weather Database (ESWD).

that decrease over time. The weak storm in contrast shows smaller Re_{BRTG51} values with no downward trend; (4) much lower environmental cloud tops (T_{TOP51}) for the severe versus weak storm and distinctly more rapid cloud top cooling for the severe storm compared to the weak storm as seen in the T_{TOP9} field. More will be said below related to the T_{TOP51}, T_{G9}, T_{1451}, and Re_{BRTG51} fields; and lastly, (5) the Tri-Spectral field shows a jump to positive values between 25 and 30 min of cloud growth, denoting cloud top glaciation [*Mecikalski et al*., 2010a].

Additional details are provided below on how a severe weather observation was associated with a given CI event, while CI was determined using radar data from the Opera radar network over Europe. For this project, 5 min resolution *Meteosat-8* IR channel observations were collected and processed into 11 CI fields, 41 T-r_e quantities, and 9 other variables (e.g., date, time, latitude, and longitude). Table 1 lists the 61 fields that were initially evaluated.

From *Meteosat* SEVIRI, channels 1.6, 3.9, 6.2, 7.3, 8.7, 10.8, 12.0, and 13.4 μm were used. The derived CI fields focused on cumulus cloud development in the 0–45 min period (ten 5 min periods), as clouds grew from the "fair weather" or cumulus *mediocris* to more towering cumulus, cumulus *congestus*, and cumulonimbus, as done in prior studies [*Mecikalski et al*., 2010a, 2010b]. For all 340 storms, CI occurred by the 45 min time of analysis. In this way, a total of 61 fields for each of the 340 studied clouds for 10 time frames (from 0 to 45 min every 5 min in *Meteosat-8* data) were collected to form our testing and training databases as used in the statistical model development. Each of the clouds were subsequently tracked and processed onward from 45 min to 2 h over 5 min periods, for a total of 25 5 min times from the CI stage/early cumulonimbus cloud, and then related to possible severe weather (high winds, large hail, and tornadoes) 2–3 h after the initial cumulus clouds formed during the CI stage of a storm. Tracking was maintained through 3 h past the CI stage in an effort to determine if severe weather was produced by a given storm. From the 2–3 h time,

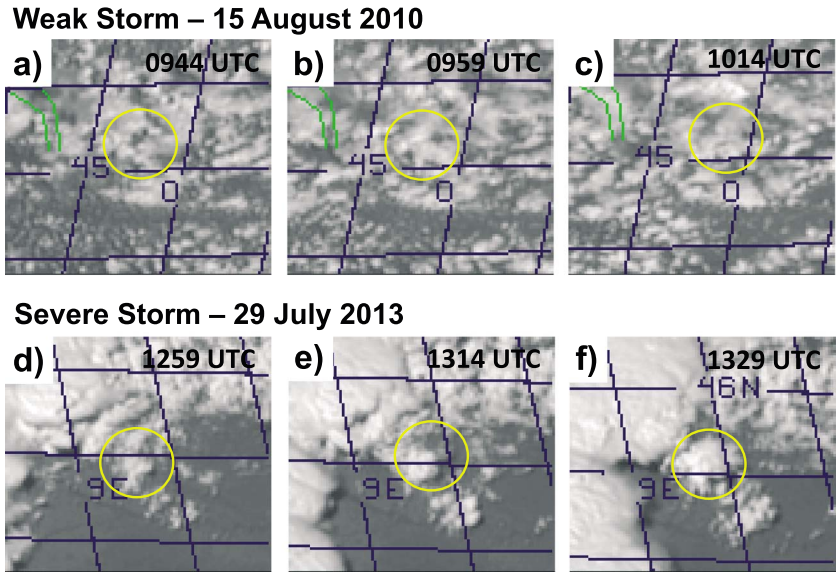

Figure 2. Examples of storm development for two cases within our 340 storm data set, (a–c) for a "weak" storm at 15 min intervals from 09:44 to 10:14 UTC 15 August 2010 and (d–f) for a "severe" storm at 15 min intervals from 12:59 to 13:29 UTC 29 July 2013. The location of the storm in Figure 2b is 45.41°N, 1.98°E, while that for the storm in Figure 2e is 45.47°N, 9.34°E. The latitude and longitude lines are every 0.5° × 0.5°.

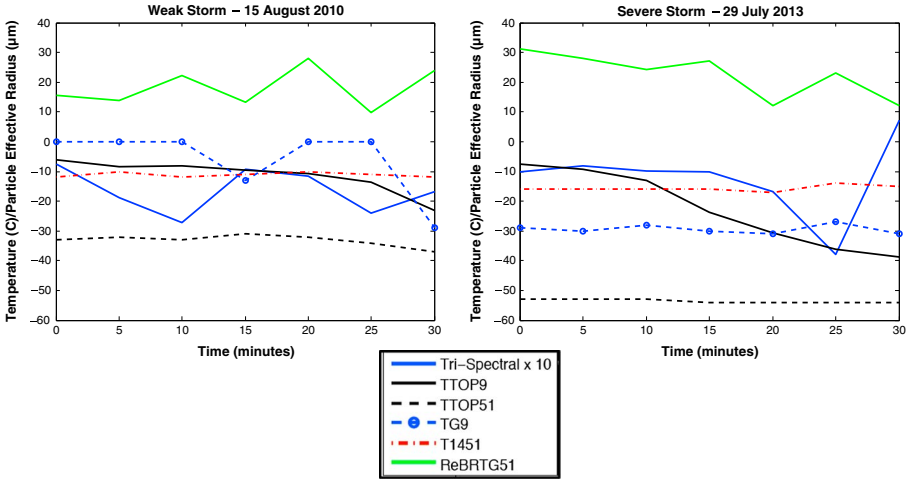

Figure 3. The 5 min trends in five T-r_e fields and the Tri-Spectral field (see Table 1) over the first 30 min of cumulus cloud development. These growing cumulus clouds are for the eventual (left) "weak" (Figures 2a–2c) and (right) "severe" storms (Figures 2d–2f). Note that the T_{G9}, T_{1451}, and Re_{BRTG51} fields are those used within equation (1) [LDA_{STORM}]. See text for the description of values and trends.

along the track of a given storm, a radius of 1.25° (139 km) was then searched for a QC2-level ESWD severe weather report in association with a given storm. By hand analysis of severe weather related to individual storms was also done to verify a storm-ESWD report association.

The work done to produce a good quality database involved considerable time, which is the reason why it was not possible to create a much larger data set. A human expert manually tracked all growing cumulus clouds over a 2 h time period to assure that cloud-tracking errors were held to a minimum (along the lines of the tracking methodology in *Lensky and Rosenfeld* [2006]), and therefore, no automated tracking was established in this exploratory study. Similarly, the T-r_e fields were manually developed for all events and also cataloged for 2 h. The CI fields were only developed in the 0–45 min time period, after which point, when a cloud formed an anvil top, they could no longer be defined since satellite fields that describe cloud growth would show no change in the presence of a more static anvil cloud. Subsequently, T-r_e fields were computed following the methodology of *Rosenfeld and Lensky* [1998], yet were often not well defined early in a cloud's lifetime especially if the cumulus clouds were isolated and if partial pixel filling did not provide valid retrievals of T and r_e.

The data processing methodology is schematically shown in Figure 4 in which three different scales in the *Meteosat-8* data were analyzed for all developing storm events: the "cloud scale" (3 × 3 IR pixel box) that covers only a small region of developing cumulus clouds during CI, the "storm scale" (9 × 9 IR pixel box) that covers a larger region as a storm grew to produce an initial anvil cloud, and the "environmental scale" (51 × 51 IR pixel box) that covers a meso-β scale (153 × 153 km) region as a means of capturing the environment in which convective storms are developing. This 51 × 51 pixel region was chosen as it corresponds to a region for which the influences of advection, convective instability, and wind shear would influence storm organization on time scales of 1–3 h [e.g., *Anthes et al.*, 1982; *Roberts et al.*, 2006]. For all domains, the coldest pixel in the 3 × 3 pixel domain defined

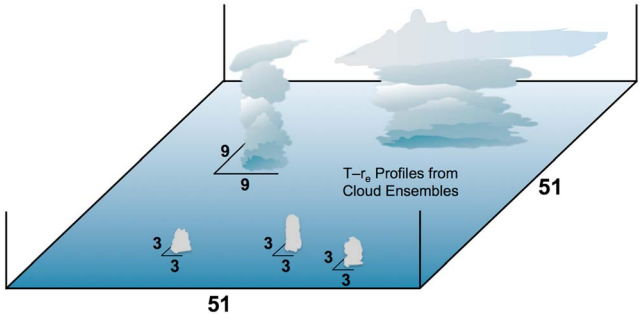

Figure 4. Schematic diagram of the *Meteosat-8* processing methodology, with a focus on 3 × 3 pixel "cloud scale" CI fields, 9 × 9 pixel "storm scale," and 51 × 51 pixel "environmental" scale. The full data processing methodology is provided in the main text.

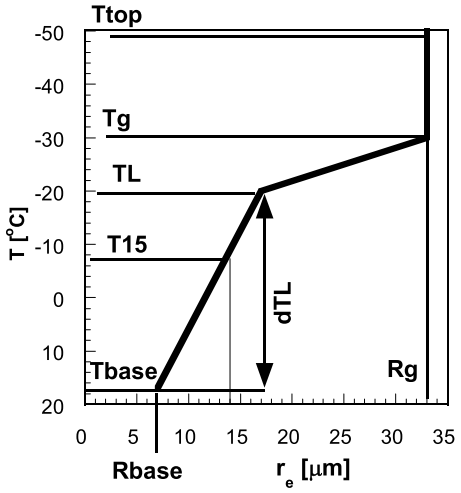

Figure 5. Illustration of the meaning of the parameters describing the temperature–particle effective radius (T-r_e) relations from *Rosenfeld et al.* [2008a]. Here T is in °C and r_e is in μm. The illustrated parameters consist of T_{base}: temperature of cloud base, approximated by the warmest point of the T-r_e relation; R_{base}: the r_e at cloud base; T_{15}: temperature where r_e crosses the precipitation threshold of 15 μm (while the 14 μm temperature is used in this study); TL: temperature where linearity of the T-r_e relation ends upward, also termed the "breakpoint"; dTL: temperature interval of the linear part of the T-r_e relation; T_g: onset temperature of the glaciated zone; R_g: the r_e at T_G; T_{TOP}: cloud top temperature.

the center pixel [see *Lensky and Rosenfeld*, 2006]. This three-tiered approach assured that CI and T-r_e fields could be computed in appropriate ways; specifically, it was not reasonable to compute T-r_e fields over 3×3 IR pixel regions since the *Rosenfeld et al.* [2008a] methodology analyzes an ensemble of cumulus clouds at various altitudes across a region toward generating a T-r_e profile, as described above. The T-r_e fields possessed increasing value as isolated clouds grew past the smaller cumulus cloud scale and as populations of cumulus clouds at varying vertical growth/development stages covered a scene such that the "space-time exchangeability" concept [*Lensky and Rosenfeld*, 2006] applied and full T-r_e profiles could be formed. Hence, moving to larger domains, 9×9 *Meteosat* pixels and especially 51×51 pixels is quite appropriate when developing T-r_e profiles and also allows for the clouds within the satellite imagery to provide information on the convective response to environmental conditions. Figure 5 presents the T-r_e fields in an idealized profile, as referred to throughout this study.

From Table 2, within the 340 storm database, 34 (10%, that is, 0.1 prior probability of having a severe event) of them later evolved to become defined severe convective storms as they produced large hail, high winds, and/or a funnel cloud according to QC2-type reports in the ESWD, per the ESWD definition of a severe storm which include having a tornado, or ≥2 cm diameter hail, and/or measured or estimated surface winds with velocities ≥25 ms^{-1}. Validation of severe classification was also attempted using satellite attributes associated with severe storms, such as the height of an overshooting top [*Bedka et al.*, 2010] and rapid cloud top expansion rates. Nevertheless, due to the high correlation between satellite-estimated classification of severe weather and many of the early cloud growth fields, the final choice was to use the "satellite-independent" ESWD severe weather reports despite the likelihood that reports were missed for several storm events and therefore do not appear in the ESWD. Thirty-four severe events within our database were associated with a QC2 ESWD report.

The time-distance criterion used to assign a severe weather event to a CI occurrence, reported within the ESWD, was that a severe weather report be within 3 h of the initial location of cumulus cloud development (i.e., our "time 0" for tracking an event or the initial CI time) and within 1.25° (139 km) from the 3 h storm location. Lowering these criteria (i.e., extending to larger time differences or distances) resulted in >34 events being classified as severe; however, the relationships to early cloud development became less well defined, especially as the time increased beyond 3 h (from time 0) or as the distance extended beyond 139 km (which resulted in severe weather reports from nearby storms perhaps becoming associated with other nonsevere events).

Given the variable list in Table 1, a first assessment of physical relationships to severe convection, the original 61 variables was reduced to 47 (the bolded fields in Table 1). The 14 fields removed were variables with too many constant values [$COOLING_9$, S (multiply9), S_{TBR9}, and S (multiply51)], too many missing values (dSLOPE9*10, COR_{TBTG9}, and T_{BRTG9}), and those fields that were not significant in this study's context (date, storm, map, hour, i_{CENTER}, and j_{CENTER}). Using these 47 variables for all events, several forms of analysis were

performed, specifically to understand the behavior of the field distribution, the evolution of fields over time (every 5 min from 0–45 min), and then to assess variable importance and initial performance in a linear statistical model.

In addition to the analysis of variable evolution, two questions were addressed: (1) what variables were more or less related to the eventual occurrence of "intense" or severe convective storms? And, (2) what subset of variables could then be used to predict whether a given area or cluster of growing cumulus clouds would become severe at some later time over the coming 2–3 h? Toward addressing these two questions, several analysis methods were applied to quantify the temporal behaviors of individual CI and T-r_e fields in the 0–45 min time frame from the beginning of an event. The statistical analysis described below had initially been performed on every individual time frame, e.g., first, all 340 "0 min" cases alone and then all "5 min" cases, etc. The scope was to understand if there is a better time step than the other, to identify the potential for severe storm development. Unfortunately, it was soon recognized that 340 storms, with only 34 severe events, were too few to develop a robust statistical model, in particular when a prognostic (two thirds of data as training sample and one third as validation/test sample) approach was applied.

In order to overcome this problem, a new, second strategy was introduced. In this second approach more time frames were aggregated together in order to increase the total number of cases. That is, in this second strategy, not only one time frame was associated with the predictand (i.e., severity of that given mature storm) but rather a sequence of more time frames (5 min cases) were associated to the same predictand, which was constant during the different time frames. In this methodology, information coming from the short-time predictor trend can also be retained. The drawback of this method is that the predictor values are not completely independent from each other, since small time steps only separate them. Hence, not as much new information is added to the original 340 event database if too few time frames were aggregated. After testing different aggregation factors, it was found a good compromise aggregating the first six time frames (from 0 min to 25 min after the first cell identification), obtaining a total of $340 \times 6 = 2040$ cases, with 204 of them marked as severe. Note that, as will be explained later, the test sample used to validate the statistical model was built using storm events and days different from those fitted during the training phase. In this way, a true independence between training and validation samples was assured.

4. Results

For this study, based on the stated goals, the first component of the analysis was to assess the field magnitudes between the occurrence or nonoccurrence of severe events, while the second component focused on the temporal evolution of the fields, specifically how the magnitudes of fields changed with time from initial CI to the formation of an anvil, and then onward to the evolution to a more mature storm by and beyond 2 h. For example, stronger events that eventually produced verified severe weather should be associated with stronger initial updrafts, and these satellite-inferred updrafts will reach a peak magnitude at some point just prior to anvil development, after which cloud top cooling trends will end (or be limited to signatures from intermittent overshooting tops). Understanding the evolution of the fields then helps in the formation of a conceptual model for using satellite indicators when defining severe (versus nonsevere) convection in a short-term prediction methodology.

4.1. T-r_e Field Delineation and Evolution Relative to Storm Intensity

Within our event database weak events were subsequently defined specifically as a cumulus cloud that never grew deep enough to have a 10.8 μm $T_B < 250$ K over the 0–45 min period of analysis. In this way, out of the initial 340 storms, 47 weak events were assigned to a storm intensity of "0." As noted, 34 severe events got an intensity value of "1" (or were associated with a QC2 ESWD report), while the remaining cases (259) were assigned to a predictand value of "0.5" (hereafter referred to as "average" storms). In the analysis of CI events across the spectrum of intensities, from the weak to severe, simple distributions of field magnitudes can be formed. The purpose of these distributions is to determine the behavior of the fields related to the physics of convective storm development, and such that one could use them in a nowcasting algorithm if specific per-field thresholds were needed. The focus of this analysis will be on the "cumulative" and "multiply" fields (Table 1) that are presented to demonstrate the progression of T-r_e fields within a growing convective cloud. Early in a cumulus cloud's development, some T-r_e fields cannot be defined, and hence, the multiply

fields will be zero. The cumulative fields will however be nonzero from the initial cloud's growth onward and increase in value. Once all T-r_e fields are defined, the multiply fields become nonzero, indicating a mature convective cloud.

Figures 6a–6f show the multiplicative and cumulative scores for both the 9×9 [S (multiply9) and S (cumulative9)] and 51×51 pixel [S (multiply51) and S (cumulative51)] domains (Table 1) as a function of time from 0 to 45 min for all storms, in which the 5 min cloud top cooling rates (5 min 10.8 μm trend) varied over six different ranges, from <-3°C per 5 min to <-18°C per 5 min. The storms were analyzed over 45 min in Figure 6 to account for the CI period plus added time for clouds to form initial anvils, which help form the full T-r_e profile. In Figures 6a–6f, the 45 min time period is presented as nine separate 5 min time periods, 1–10. The score fields are useful as a means of assessing the overall value of the T-r_e fields in delineating overall storm intensity. Several interesting features are evident: (1) the multiplied scores on the 51×51 domain were nonzero only from times 2–7 (5–30 min), (2) the multiplied scores on the 9×9 domain were nonzero at the initial and the last 2 times (40 and 45 min), (3) the cumulative scores on the 51×51 domain gradually decreased after time 7 (30 min) and were seen to increase from 1.5 to near 2.5 from the <-3 to <-18 events, and (4) the cumulative scores on the 9×9 domain generally remained in the 2.0–2.5 range and also increased by ~10% between the weakest and strongest 10.8 μm T_B cooling rate events. The behavior of the 9×9 multiplied score is due to the need for all fields that comprise the score to be nonzero, or that a mature, large (comprising several 3 km IR pixels) cumulus cloud be present that exhibits significant cloud top glaciation and growth, which only happened after time 8 (35 min).

The next components of this study involved assessing the relative importance of the 47 variables and then to determine how best to use a subset of these fields to predict at early stages of cloud growth future storm intensity.

4.2. Predictor Variable Importance and Model Development

The first statistical method applied in the study was a *regression* method. Using the weak, "average," and severe event definitions of storm intensity, the database was processed with the "leaps" package in the *R Project for Statistical Computing* (www.r-project.org) to perform an exhaustive search for the best subsets of the candidate variables in a vector X for predicting an outcome Y (storm intensity) with a linear regression, using an efficient branch-and-bound algorithm. Results from this regression study showed that the total number of cases, even after aggregating six time frames together, were not sufficient to give significant results on the independent test data set. Moreover, the weak events were not statistically independent from all the satellite fields (by definition) and that introduced spurious correlation between some predictors and the predictand. So that method was abandoned because the definition of weak events was based on the value of some predictors, which is misleading.

The second statistical method used was a *classification* method based on simple linear discriminant analysis (LDA) and also implemented in the *R* language to discriminate the severe events (labeled as class 1) from all the other events (all labeled as class 0). The database developed here was shown to be sufficient to perform a bivariate analysis, useful to compare the different candidate predictor performances, and also sufficient for a simple prognostic multivariate approach, joining together two or three predictors. After initial attempts were made to use nonlinear models to assess variable importance, several more simple evaluations were done using a *bivariate* LDA. When looking for the predictor "best threshold" to discriminate between two classes, many different verification scores could be optimized. It was decided to maximize the Peirce skill score ("maxPSS"), following that suggested by *Manzato* [2007]. Prior to performing the LDA, the data sets were combined over the first six time periods (from 0 to 25 min) of cloud growth, forming then a larger database toward understanding how early cloud growth signatures relate to later storm intensity (as described above).

Within the bivariate LDA framework, a simple diagnostic procedure was performed, i.e., without dividing the database in training and validation. Results for the first best 11 predictors are shown in Table 3. All other predictors have maxPSS lower than 0.13. The best two predictors from this diagnostic bivariate LDA are T_{G9} and T_{1451} that correspond to the response of cloud microphysical character to the presence of a strong in-cloud updraft, along the lines of *Lensky and Rosenfeld* [2006] and *Rosenfeld et al*. [2008a, 2008b]. Rapid cloud growth corresponds to a delay in particle growth, leading to colder temperatures of the first 14 μm particles and also lower T_G values (owing to smaller particles freezing at temperatures closer to the homogenous freezing point of water [*Rosenfeld and Woodley*, 2000]).

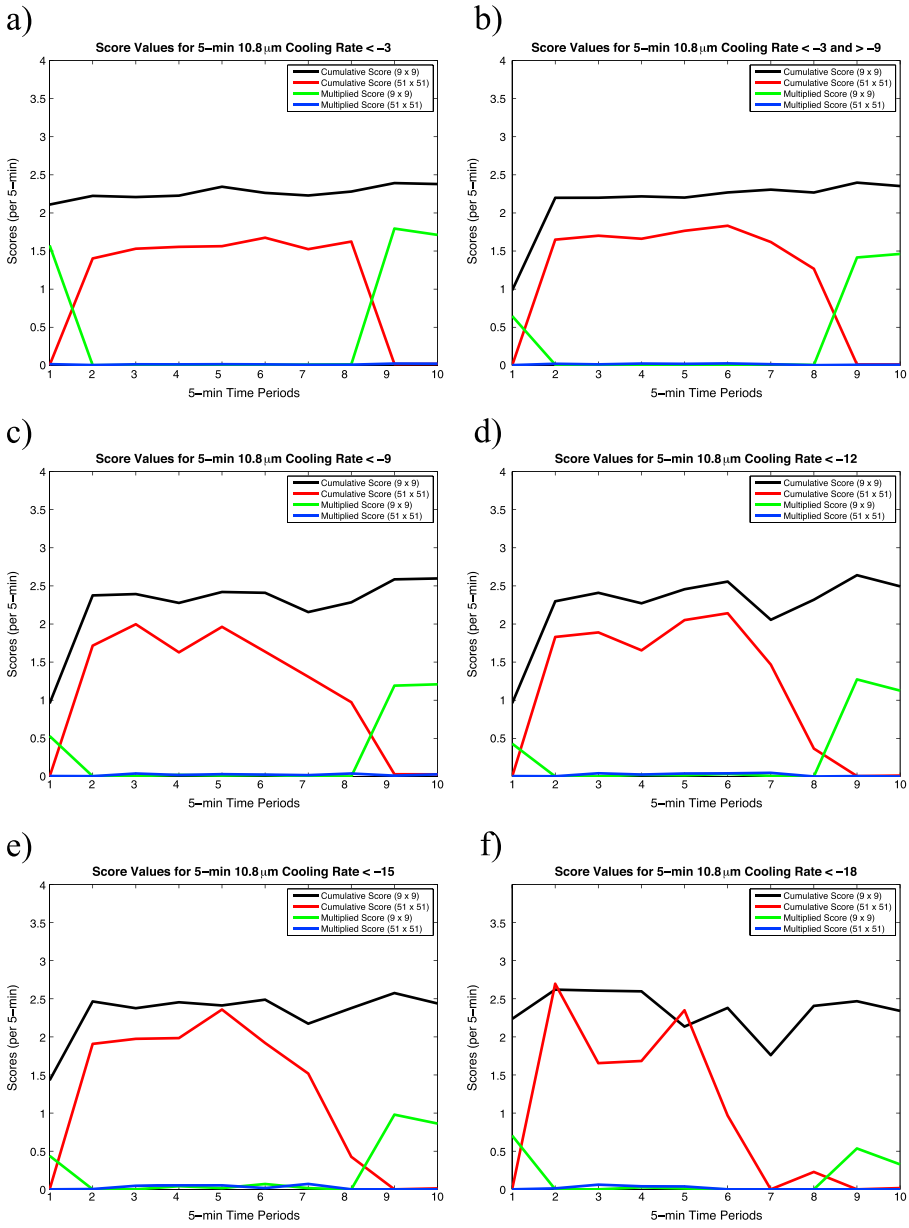

Figure 6. Score values for "cumulative on the 9 × 9 pixel domain," "cumulative on the 51 × 51 pixel domain," "multiplied scores on the 9 × 9 pixel domain," and "multiplied scores on the 51 × 51 pixel domain" for clouds with varying 5 min cloud top cooling rates, from (a) <-3°C to (f) <-18°C. Here "score" refers to the cumulative score (whether summed or multiplied) on the 9 × 9 pixel "storm scale" or 51 × 51 "environmental scale," of the five fields S_{dSLOPE}, S_{TG}, S_{TBR}, S_{REG}, and S_{REBR}, as defined in Table 1. In Table 1, these summed or multiplied fields are *S* (cumulative9), *S* (cumulative51), *S* (multiply9), and *S* (multiply51). See text for interpretation of results.

Variable "importance" is a concept very well defined in bivariate analysis, where after choosing a performance "metric," it is easy to rank each variable's goodness according to that specific metric. But, variable importance is a much more complex concept when doing a *multivariate* analysis, because different variables that, when taken alone, may have high performances, and model performance may not increase when different variables are used together. Highly correlated variables (even nonlinearly) do not bring new independent information into a multivariate model but rather risks introducing noise into the results.

In our database, many satellite-derived candidate predictors have high correlations. Notable examples include Re_{GLAC9} and S_{REG9} ($R = -0.98$), Re_{BRTG9} and S_{REBR9} ($R = -0.90$), T_{G9} and S_{TG9} ($R = -0.85$), and T_{149}

Table 3. The 11 Best Predictors of a Simple Diagnostic Bivariate Analysis

Predictor	Cases Not Missing	Discriminant Condition	maxPSS
T_{G9}	2040	<-24.6	0.22
T_{1451}	2014	<-17.0	0.22
S_{TG9}	2040	>0.16	0.21
T_{TOP51}	2040	<-47.8	0.19
Re_{TOP51}	2040	<36.6	0.18
S_{REG9}	2040	<0.88	0.18
T_{TOP9}	2040	<-28.9	0.17
T_{B9}	2040	<-6.9	0.16
Re_{GLAC51}	1776	<31.3	0.16
T_{149}	1961	<23.0	0.15
Re_{BRTG51}	2040	<21.8	0.15

and T_{B9} ($R = 0.83$). For this reason, in a multivariate approach it is important to implement a strategy for selecting a small subsample of *statistically independent* predictors, because too many predictors could introduce noise and increase data *overfitting*. In order to avoid overfitting, the original database was divided in training and test samples. Since different clouds of the same day could have been close in space to each other and hence very similar, it was decided to use all clouds of three specific days (1 July 2012, 7 July 2012, and 29 July 2013, for a total number of 648 cases) to form the "test sample," while all the cases from the remaining 3 days formed the "training sample" (having a total of 1392 cases). In such a way a true independence of the test sample was obtained.

Prior studies have suggested preprocessing the predictors before developing a multivariate statistical model. This is particularly true when the model parameters are found by iterative approximations, starting from random initialization, as done in nonlinear methods. For example, *Masters* [1995] states that "…*most nonlinear models implicitly or explicitly assume that variables having large variation are more important than variables having small variation*." But, preprocessing can be very important also in linear classification methods, when the relation between each predictor and the event occurrence is nonmonotonic. As discussed in *Manzato* [2007], transforming each candidate predictor into its empirical posterior probability (EPP) is an optimal "preprocessing" technique, in particular for nonmonotonic variables, because, when performing this transformation, all transformed variables have the same meaning and domain; that is, all of them represent their probability (0,1) of having an event occurrence. As described in *Manzato* [2005], and also done in this study, the original candidate predictor values were transformed into their EPP of having a severe event. In practice, each predictor domain is divided in 21 equal bins and the EPP transformation is obtained by fitting the ratio between the number of severe event cases and the total number of cases inside each bin of the predictor distribution domain. Examples of the EPP transformation are shown in Figures 7a and 7b, for the T_{1451} (Figure 7a) and Re_{BRTG51} (Figure 7b) predictor variables. While the Re_{BRTG51} transformation is quite linear, the T_{1451} is much more peculiar, being nonmonotonic. Figure 7 provides us information on how the different candidate predictors (spanning very different domain ranges) could be nonlinearly and nonmonotonically transformed into probabilities, that are much more comparable and hence are easier to combine together in a multivariate statistical model.

After this variable preprocessing, a prognostic bivariate analysis was performed. Instead of looking for the best threshold for each variable, a probability threshold of 0.10 (same as the severe weather *prior* probability) was chosen for all the predictors transformed into their EPP. The only six variables having a test maxPSS equal or larger than a minimum PSS threshold (set to 0.10) are listed in Table 4. In Table 4, two highly correlated predictors are seen (S_{REG9} and S_{TG9} are very correlated with T_{G9}). After removing them, the best predictors were the posterior probability associated to T_{1451} and T_{G9}, followed by those associated to T_{TOP51} and Re_{BRTG51}. The physical reasons for the importance of these variables are along the lines of that already stated above (for T_{1451} and T_{G9}), while low T_{TOP51} values imply the presence of already deep convective clouds in the mesoscale region of developing cumulus clouds. The physical relationship between severe weather and the Re_{BRTG51} variable is that strong updrafts produce microphysical particles with anomalously small sizes, as compared to what occurs in more common convective clouds [*Rosenfeld et al*., 2008a].

Next, it was decided to use an exhaustive search of all the possible combinations of these four variables that are six combinations of two of them, four combinations of three of them, and one combination using all four variables. Out of all these 11 different multivariate prognostic models, the variable subsets chosen by the 4 models showing the best performances are listed in Table 5. Considering the performances in Table 5, it is possible to see that the last two LDA models are slightly overfitting the training data set (training score significantly

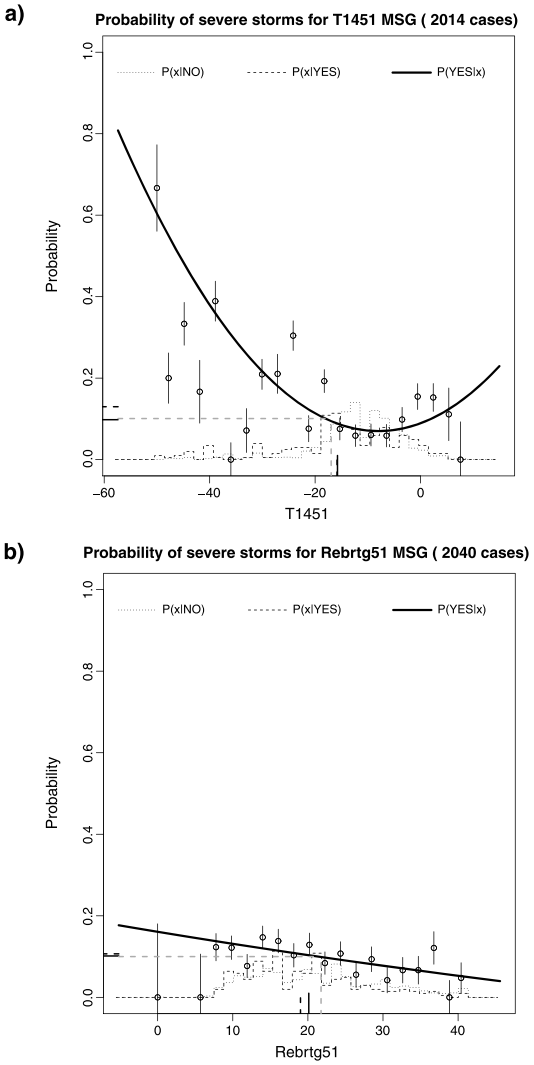

Figure 7. Examples of the EPP transformation for (a) the T_{1451} and (b) Re_{BRTG51} predictor variables. See text for description of results.

larger than the test score). For that reason the second model was chosen to illustrate in more details the performance obtained (bold "0.31" in Table 5). That model can be described by the following equation:

$$\begin{aligned} LDA_{STORM} = {} & 18.205\ EPP(T_{G9}) \\ & + 8.293\ EPP(T_{1451}) \\ & + 21.164\ EPP(Re_{BRTG51}). \end{aligned} \quad (1)$$

Severe weather is expected if $LDA_{STORM} \geq 4.755$.

Considering Figure 8 as an illustration of the LDA posterior probability versus LDA_{STORM}, i.e., the model output of equation (1), it is possible to see that the discriminant threshold (4.755) that maximizes the PSS of the classification model corresponds to a posterior probability of event occurrence equal to 0.08. Apart from the optimized score (maxPSS), other more commonly used classification performances are reported (following the definitions of *Jolliffe and Stephenson* [2003]) in Table 6, for the training and test samples, respectively.

As expected for rare events (remember that in our problem the prior probability is only 0.1), maximizing the PSS leads to an overforecast; that is, the frequency BIAS is larger than 1 (4.7 and 3.8, respectively, with respect to the training and test samples, as shown in Table 6). This is due to the fact that PSS penalizes much more the "rare events" than the "very frequent" nonsevere storm events, as in the case for the present study. Toward seeing how the model performance varies with respect to the chosen 4.755 threshold, consider the situation with a BIAS = 1, which is very informative to then analyze the relative operating characteristic (ROC) diagram [*Swets*, 1973], shown in Figure 9. From this ROC figure it is possible to see that the three-variable model described in equation (1) does not suffer of an overfitting problem (test and training ROC lines overlap), which should be the first concern with any statistical model. Therefore, equation (1) can be considered a useful way to diagnose and predict near-term (0–3 h) severe convective storm development when early cloud growth (0–25 min) satellite-based cloud observations are considered.

Table 4. Maximum Pierce Skill Score (maxPSS) for the Training and Test Sample in a Prognostic Bivariate Analysis as Developed in This Study

Transformed Predictor	Training maxPSS	Test maxPSS
EPP (T_{TOP51})	0.27	0.13
EPP (T_{1451})	0.26	0.21
EPP (T_{G9})	0.20	0.24
EPP (S_{TG9})	0.20	0.22
EPP (Re_{BRTG51})	0.19	0.10
EPP (S_{REG9})	0.14	0.23

It is important to note that equation (1) applies to the *Rosenfeld et al.* [2008a, 2008b] T-r_e framework as a means of combining T_{G9}, T_{1451}, and Re_{BRTG51}. Prior to applying equation

Table 5. Maximum Pierce Skill Score (maxPSS) for the Training and Test Sample in a Prognostic Multivariate Analysis as Developed in This Study[a]

Variables Used	Training maxPSS	Test maxPSS
EPP (T_{G9}) + EPP (T_{1451})	0.27	0.25
EPP (T_{G9}) + EPP (T_{1451}) + EPP (Re_{BRTG51})	0.29	**0.31**
EPP (T_{1451}) + EPP (T_{TOP51}) + EPP (Re_{BRTG51})	0.35	0.28
EPP (T_{G9}) + EPP (T_{1451}) + EPP (T_{TOP51}) + EPP (Re_{BRTG51})	0.36	0.27

[a]The bolded "0.31" maxPSS delineates the best combination of three predictors, which forms the linear discriminant analysis (LDA) prediction model (equation (1)).

(1) for LDA_{STORM}, the EPP transformation needs to be applied to the original values as

$$\mathrm{EPP}(T_{G9}) = 0.058 - 0.00175 \times T_{G9}, \tag{2}$$

$$\mathrm{EPP}(T_{1451}) = 0.069 + 0.00030 \times (T_{1451} + 8)^2, \tag{3}$$

$$\mathrm{EPP}(Re_{BRTG51}) = 0.087 + 0.01220 \times \mathrm{ATAN}\ (1.005 + 0.970 \times Re_{BRTG51}). \tag{4}$$

Once done, equation (1) can be computed and a comparison to the 4.755 threshold is made in order to forecast severe or not severe events.

As an example, Figure 10 shows the LDA_{STORM} distribution for all 34 severe storm and all 305 nonsevere events (sum is only 339 cases because one nonsevere case had missing T_{1451}), taken 25 min after first CI identification (one frame only analysis). Note that for Figure 10 there is no division in training/validation, so also, the cases used to develop the model are included. Table 7 shows the corresponding contingency table, obtained using the 4.755 threshold. Figure 10 and Table 7 demonstrate what a forecaster would see from the analysis of satellite imagery 25 min after CI initiation through the application of the model given by equation (1).

5. Conclusions

The study presented here examined the characteristics and importance of 47 satellite-based fields from the *Meteosat-8* geostationary satellite over Europe that describe growing convective clouds (CI fields) and cloud top microphysics (so-called T-r_e fields) for a range of storm intensities. The main goal of this study was to determine the unique signatures in the early growth stages of cumulus clouds for storms that later produced a severe weather report and contrast them with storm signatures that did not produce severe weather. A follow-on goal was to develop a simple model using significant satellite fields to help predict which storms will become severe over the coming 2–3 h after CI. A total of 340 convective storm clouds were examined, from the cumulus cloud/early growth stage (0–45 min) on to the more mature cumulonimbus cloud stage (from 45 min to 2 h), over central Europe on 6 days from 2010 into 2013. Within this sample data set, 34 convective storms were associated with a QC2-quality severe weather report in the ESWD. A severe weather event was either a report of large hail, high surface winds, or a tornado. Each convective storm was examined using 5 min resolution *Meteosat-8* IR channel data, and as a result, a total of 3400 cases (or individual times) were available for analysis.

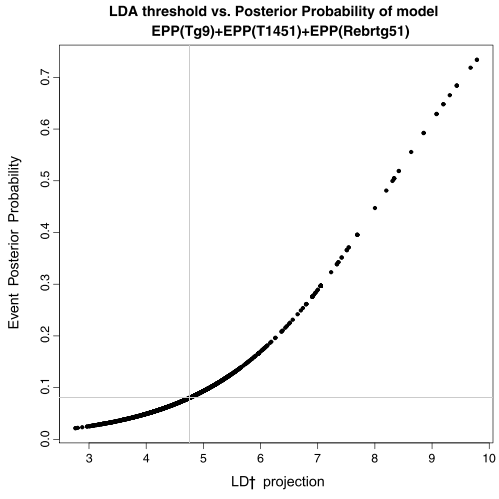

Figure 8. Illustration of the LDA threshold versus LDA_{STORM}, i.e., the output of model in equation (1), as described in text.

Table 6. Contingency Table and Derived Scores for the Three-Variable Model of Equation (1) Computed on the Training and Test Samples[a]

Training Sample	
Contingency table	
A 93 B 517	
C 38 D 718	
Derived scores	
POD = 0.71	Probability of detection: forecasted events really happened over total events
HIT = 0.59	HIT rate: forecasted event/nonevent over total cases
FAR = 0.85	False alarm ratio: forecasted event not really happened
POFD = 0.42	Probability of false detection: false alarm over total nonevents
BIAS = 4.66	Forecasted events over total events
TS = 0.14	Threat score: forecasted events really happened over total forecast less no cases
HSS = 0.11	Heidke skill score: forecast system over random system
PSS = 0.29	Peirce (Kuipers) skill score: forecast system over climatology
ODDS = 3.40	Odds ratio
Test Sample	
Contingency table	
A 50 B 221	
C 22 D 355	
Derived scores	
POD = 0.69	Probability of detection: forecasted events really happened over total events
HIT = 0.63	HIT rate: forecasted event/nonevent over total cases
FAR = 0.82	False alarm ratio: forecasted event not really happened
POFD = 0.38	Probability of false detection: false alarm over total nonevents
BIAS = 3.76	Forecasted events over total events
TS = 0.17	Threat score: forecasted events really happened over total forecast less no cases
HSS = 0.14	Heidke skill score: forecast system over random system
PSS = 0.31	Peirce (Kuipers) skill score: forecast system over climatology
ODDS = 3.65	Odds ratio

[a]For the training sample, there are 1392 different cases, with 26 forecast missing values, with the total evaluated cases being 1366. For the test sample, there are 648 different cases, with 0 forecast missing values, and the total evaluated cases being 648.

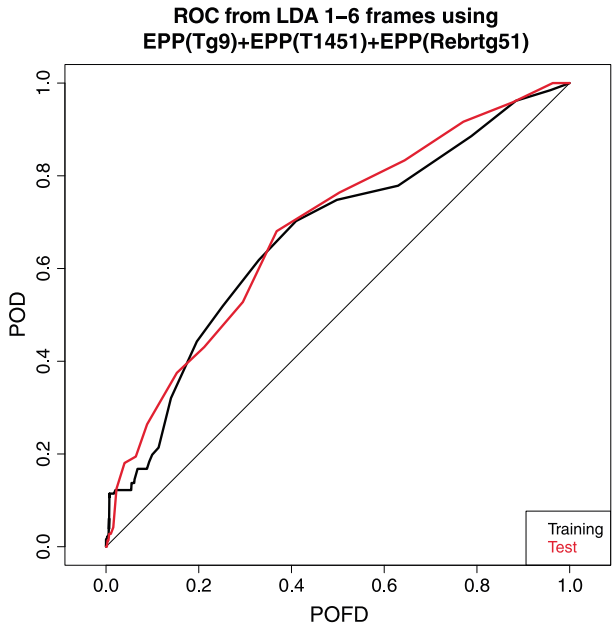

Figure 9. Receiver operating characteristic (ROC) curve for the linear discriminant analysis model with three predictors, cloud top glaciation temperature on the 9 × 9 pixel "storm scale" (T_{G9}), the minimum temperature where the 14 μm particle size occurs over the "environment scale" (T_{1451}), and the particle effective radius at the breakpoint of the T-r_e line (Re_{BRTG51}).

Beginning with 47 satellite variables, several approaches were used to (1) determine where nonredundant information existed across variables and (2) identify a small subset of fields that could be applied within a short-term satellite-based prediction algorithm. These goals were accomplished in part using a prognostic approach, that is, by dividing the entire data set of cases into training and testing samples. The present study stopped short of applying the LDA_{STORM} model to a new, larger set of storm cases, or to apply to model to a real-time data set, which is the subject of a follow-on research project.

The main conclusions are summarized as follows: (1) rapidly growing cumulus clouds in advance of a severe storm exhibit unique (i.e., very low to below −25°C) glaciation temperatures (T_{G9}) compared to when only rain showers occur. (2) The environmental/meso-β scale (51 × 51

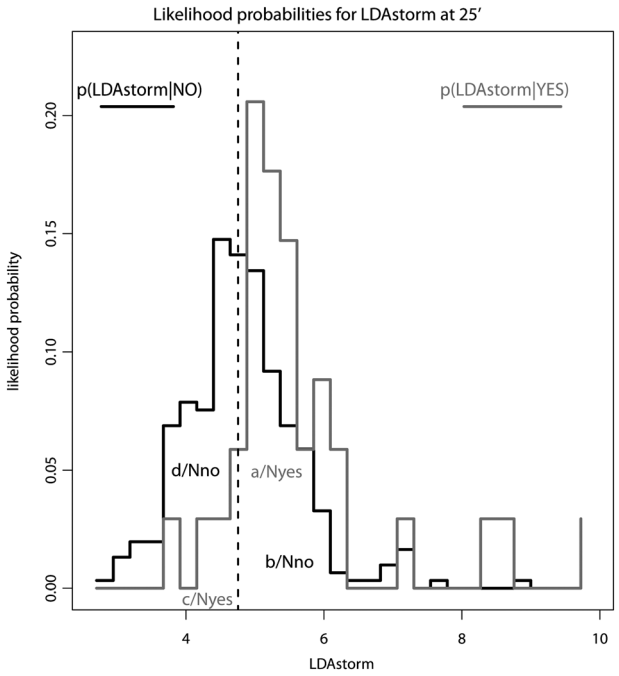

Figure 10. Distribution of LDA_{STORM} values computed using equation (1) (and EPP transforms in equations (2)–(4)) for the 340 storm data set used in this study at frame 6 (25 min after CI). Solid line is the likelihood probability for the nonsevere cases, gray line is the likelihood probability for the 34 severe cases, and the dashed line is the threshold found to maximize PSS during the model development. Note that there is no division in training/validation, so also the cases used to develop the model are included. The "*a*," "*b*," "*c*," and "*d*" variables are the contingency table coefficients, and "Nyes" and "Nno" are the number of observed event and nonevent cases. This figure demonstrates the skill of a forecasting method based on the analysis at 25 min after CI of satellite imagery through the model of equation (1).

pixel region)/cloud ensemble or arithmetic average of the temperature where the 14 μm particles (T_{1451}) are first seen are also unique, implying that precipitation begins at higher altitudes when updrafts are stronger in advance of severe storms. (3) The environmental/meso-β scale (51 × 51 pixel region)/cloud ensemble or arithmetic average r_e values at the T-r_e sounding breakpoint temperature (Re_{BRTG51}) noting that stronger updrafts produce microphysical particles with anomalously small sizes, as compared to what occurs in more common convection. Again, Figure 3 shows the behavior of these three fields for one weak and severe storm event.

The three variables chosen for the final model are the empirical posterior probability of T_{G9}, T_{1451}, and Re_{BRTG51}. As noted above, the physical reasons for the importance of these variables are that strong storms will have anomalously low temperatures (5–10°C colder than surrounding storms) where the first 14 μm particle (T_{1451}) and where particles first freeze (T_{G9}). The physical relationship between severe weather and the Re_{BRTG51} variable is that strong updrafts produce microphysical particles with anomalously small sizes and especially trends to lower r_e values, as compared to what occurs in more average convection. The performances of the three-variable statistical LDA model (equation (1)), illustrated by Figures 9 and 10 and by Tables 6 and 7, may not be sufficiently high for an operational implementation of that model, but the statistical methodology implemented in this work should give much better results once a larger data set could be provided via an automated tracking procedure,

Table 7. Contingency Table and Derived Scores for the Three-Variable Model of Equation (1) Computed on All the 339 Cases at Frame 6 That Is 25 min After CI Identification[a]

All Cases at 25 min	
Contingency table	
A 30 B 143	
C 4 D 162	
Derived scores	
POD = 0.88	Probability of detection: forecasted events really happened over total events
HIT = 0.57	HIT rate: forecasted event/nonevent over total cases
FAR = 0.83	False alarm ratio: forecasted event not really happened
POFD = 0.47	Probability of false detection: false alarm over total nonevents
BIAS = 5.09	Forecasted events over total events
TS = 0.17	Threat score: forecasted events really happened over total forecast less no cases
HSS = 0.15	Heidke skill score: forecast system over random system
KSS = 0.41	Kuipers skill score: forecast system over climatology
ODDS = 8.50	Odds ratio

[a]These data include also those used to develop the statistical model.

that is, the scope of future works, which will involve the use of much larger training and testing databases, on the order of thousands of events in size, and incorporating information from operational numerical weather prediction models (e.g., the high-resolution rapid refresh) for environmental conditions.

Given the general degree of nonuniqueness seen when evaluating field differences across storm intensity, this study likely shows the practical limitations of using 2–4 km resolution IR data from *Meteosat* and other geostationary satellites when nowcasting severe storms in the 1–2 h time frame, something that will be improved as the spatial resolution on geostationary satellites improve over time. However, the improved satellite-based CI nowcasts that utilize statistical learning models can be employed within existing systems that monitor and track convection for a variety of users. Use of the methods described here will afford an added capability to not only nowcast CI but also provide predictions for which storms will later become severe, following on the study by *Rosenfeld et al*. [2008b]. Short-term prediction systems that can be improved by such enhanced satellite-based information on growing cumulus clouds include the GOES-R 0–1 h CI algorithm [*Mecikalski et al*., 2015], the Corridor Integrated Weather System [*Iskenderian et al*., 2010, 2012], CbTRAM [*Zinner et al*., 2008], and the Rapidly Developing Thunderstorm [*Autones*, 2012]. Similarly, the AutoNowcaster [*Mueller et al*., 1993, 2003; *Wilson et al*., 2010; *Roberts et al*., 2012] for CI and storm predictions; the Collaborative Adaptive Sensing of the Atmosphere Distributed Collaborative Adaptive Sensing network [*Ruzanski et al*., 2011] for storm cell evolution and tracking; the Warning Decision Support System–Integrated Information [*Lakshmanan et al*., 2007] Thunderstorm Identification, Tracking, Analysis, and Nowcasting [*Dixon and Wiener*, 1993] algorithm; the Canadian Radar Detection System [*Joe et al*., 2003]; and the Thunderstorm Strike Probability Nowcasting Algorithm [*Dance et al*., 2010] are systems that could be enhanced using added satellite data-processing rules. The Global/Regional Assimilation and Prediction System–Severe Weather Forecast Tool [*Hu et al*., 2007; *Wilson et al*., 2010], which processes fields from NWP models as a means of forming high-quality analyses and modeled initial conditions [*Feng et al*., 2007], may significantly benefit from the inclusion of the satellite-based fields discussed in this study, for storm initiation and tracking purposes. Subsequently, results from this study may help further our understanding of the dynamic CI process, which is of high interest [*Wilson et al*., 1998; *Ziegler et al*., 2007; *Lima and Wilson*, 2008; *Wakimoto and Murphey*, 2009], especially given the correspondence between correct short-term forecasts of convective storms and overall NWP forecast skill [*Brooks et al*., 1992].

Another important future goal is to apply this research to the *GOES-R* generation of geostationary satellites and the Advanced Baseline Imager data set as well as to the Meteosat Third Generation (MTG) Flexible Combined Imager (FCI). For *GOES-R*, these improvements fall into four themes: (1) increased visible channel resolution to 500 m, IR spatial resolution to 2 km, and increased time resolution to 5 min will help automated algorithms discern cumulus clouds better than is possible with the current GOES satellites. This increased resolution will afford enhanced nowcast lead times for CI. Furthermore, the use of 5 min resolution data will improve the tracking of small-scale cumulus clouds. The higher temporal resolution will also facilitate improved measures of the rates of change of cloud properties, which should further increase CI nowcast accuracy. (2) The additional channels (16 versus the present-day 4) will help improve our ability to determine cloud top glaciation and forming of $T\text{-}r_e$ retrievals. Having the 8.5 and 12.3 μm channels, as well as three water vapor channels (6.19, 6.95, and 7.34 μm, instead of just the 6.5 μm channel) will greatly improve our ability to detect ice versus water particles [see, e.g., *Strabala et al*., 1994]. The added 10.35 μm channel on *GOES-R* (in addition to 11.2 μm) will also improve estimates of cloud height. All of these will be critical satellite indicators of rapidly growing, deep convection. The MTG FCI will possess 1 km resolution IR channels and therefore assist in the early detection of convective clouds. Lastly, *GOES-R* will provide 30 s resolution data, with MTG providing 2.5 min resolution fields, data sets that will be used when nowcasting CI and detecting early signature of severe storms.

Acknowledgments

This project was supported by a grant from the European Organisation for the Exploitation of Meteorological Satellites (EUMETSAT), with sponsor Marianne König. Three anonymous reviewers provided considerable help toward improving the quality of this manuscript. All of the data used in this study are available from the first author, John R. Mecikalski. Please contact him by e-mail at john.mecikalski@nsstc.uah.edu for any data requests.

References

Anthes, R. A., Y. Kuo, S. G. Benjamin, and Y. Li (1982), The evolution of the mesoscale environment of severe local storms: Preliminary modeling results, *Mon. Weather Rev.*, *110*, 1187–1213.

Autones, F. (2012), Product user manual for "*Rapid development thunderstorms*" (RDT-PGE11 v3.0d). Meteo France, The EUMETSAT Network of Satellite Application Facilities, 27 pp.

Bedka, K., J. Brunner, R. Dworak, W. Feltz, J. Otkin, and T. Greenwald (2010), Objective satellite-based detection of overshooting tops using infrared window channel brightness temperature gradients, *J. Appl. Meteorol. Climatol.*, *49*, 181–202.

Bedka, K. M., and J. R. Mecikalski (2005), Application of satellite derived atmospheric motion vectors for estimating mesoscale flows, *J. Appl. Meteorol.*, *44*, 1761–1772, doi:10.1175/JAM2264.1.

Bedka, K. M., C. S. Velden, R. Petersen, and J. R. Mecikalski (2009), Statistical comparisons between satellite-derived atmospheric motion vectors, rawinsondes, and NOAA wind profiler observations, *J. Appl. Meteorol. Climatol.*, *48*, 1542–1561.
Berendes, T. A., J. R. Mecikalski, W. M. Mackenzie, K. M. Bedka, and U. S. Nair (2008), Convective cloud detection in satellite imagery using standard deviation limited adaptive clustering, *J. Geophys. Res.*, *113*, D20207, doi:10.1029/2008JD010287.
Brooks, H. E., and N. Dotzek (2007), The spatial distribution of severe convective storms and an analysis of their secular changes, in *Climate Extremes and Society*, edited by H. F. Diaz and R. Murnane, pp. 35–53, Cambridge Univ. Press, New York.
Brooks, H. E., C. A. Doswell III, and R. A. Maddox (1992), On the use of mesoscale and cloud-scale models in operational forecasting, *Weather Forecasting*, *8*, 120–132.
Brooks, H. E., C. A. Doswell, and M. P. Kay (2003), Climatological estimates of local daily tornado probability for the United States, *Weather Forecasting*, *18*, 626–640.
Browning, K. A., and D. Atlas (1965), Initiation of precipitation in vigorous convective clouds, *J. Atmos. Sci.*, *22*, 678–683.
Changnon, S. A. (2001), Damaging thunderstorm activity in the United States, *Bull. Am. Meteorol. Soc.*, *82*, 597–608.
Cintineo, J. L., M. J. Pavolonis, J. M. Sieglaff, and A. K. Heidinger (2013), Evolution of severe and nonsevere convection inferred from GOES-derived cloud properties, *J. Appl. Meteorol. Climatol.*, *52*, 2009–2023.
Cintineo, J. L., M. J. Pavolonis, J. M. Sieglaff, and D. T. Lindsey (2014), An empirical model for assessing the severe weather potential of developing convection, *Weather Forecasting*, *29*, 639–653.
Curran, E. B., R. L. Holle, and R. E. López (2000), Lightning casualties and damages in the United States from 1959 to 1994, *J. Clim.*, *13*, 3448–3464.
Dance, S., E. Ebert, and D. Scurrah (2010), Thunderstorm strike probability nowcasting, *J. Atmos. Oceanic Technol.*, *27*, 79–93.
Diaz-Uriarte, R., and A. S. de Alvarez (2006), Gene selection and classification of microarray data using random forest, *BMC Bioinf.*, *7*, 3.
Dixon, M., and G. Wiener (1993), TITAN: Thunderstorm Identification, Tracking, Analysis, and Nowcasting—A radar-based methodology, *J. Atmos. Oceanic Technol.*, *10*, 785–797.
Dixon, P., A. Mercer, J. Choi, and J. Allen (2011), Tornado risk analysis: Is Dixie Alley an extension of Tornado Alley?, *Bull. Am. Meteorol. Soc.*, *92*, 433–441.
Dotzek, N., P. Groenemeijer, B. Feuerstein, and A. M. Holzer (2009), Overview of ESSL's severe convective storms research using the European Severe Weather Database ESWD, *Atmos. Res.*, *93*, 575–586.
Evans, J. E., and E. R. Ducot (2006), Corridor Integrated Weather System, *Lincoln Lab. J.*, *16*, 59–80.
Feng, Y., Y. Wang, T. Peng, and J. Yan (2007), An algorithm on convective weather potential in the early rainy season over the Pearl River Delta in China, *Adv. Atmos. Sci.*, *24*, 101–110.
Fritsch, J. M., et al. (1998), Quantitative precipitation forecasting: Report of the Eighth Prospectus Development Team, U.S. Weather Research Program, *Bull. Am. Meteorol. Soc.*, *79*, 285–299.
Hamill, T. M., and A. T. Church (2000), Conditional probabilities of significant tornadoes from RUC-2 forecasts, *Weather Forecasting*, *15*, 461–475.
Harris, R. J., J. R. Mecikalski, W. M. MacKenzie, P. A. Durkee, and K. E. Nielsen (2010), The definition of GOES infrared lightning initiation interest fields, *J. Appl. Meteorol. Climatol.*, *49*, 2527–2543.
Hartung, D. C., J. M. Sieglaff, L. M. Cronce, and W. F. Feltz (2013), An intercomparison of UW cloud-top cooling rates with WSR-88D radar data, *Weather Forecasting*, *28*, 463–480.
Heidinger, A. K., and M. J. Pavolonis (2009), Gazing at cirrus clouds for 25 years through a split window. Part I: Methodology, *J. Appl. Meteorol. Climatol.*, *48*, 1100–1116, doi:10.1175/2008JAMC1882.1.
Hosmer, D. W., and S. Lemeshow (1989), *Applied Logistic Regression*, 307 pp., John Wiley, New York.
Hu, S., S. Gu, X. Zhuang, and H. Luo (2007), Automatic identification of storm cells using Doppler radars, *Acta Meteorol. Sin.*, *21*, 353–365.
Iskenderian, H., C. F. Ivaldi, M. Wolfson, J. R. Mecikalski, K. M. Bedka, J. Sieglaff, W. Feltz, R. Dworak, and W. M. MacKenzie (2010), Satellite data applications for nowcasting of convective initiation, in *14th Conference on Aviation, Range, and Aerospace Meteorology*.
Iskenderian, H., L. Bickmeier, J. Mecikalski, and C. P. Jewett (2012), Satellite data applications for nowcasting of cloud-to-ground lightning initiation, Proc. *18th Conf. on Satellite Meteorology, Oceanography and Climatology/ First Joint AMS-Asia Satellite Meteorology Conference*, New Orleans, La., 22–25 Jan.
Joe, P., M. Falla, P. V. Rijn, L. Stamadianos, T. Falla, D. Magosse, L. Ing, and J. Dobson (2003), Radar data processing for severe weather in the national radar project of Canada, Preprints, 21st Conf. on Severe Local Storms, San Antonio, Tex., Am. Meteorol. Soc., P4.13. [Available online at http://ams.confex.com/ams/pdfpapers/47421.pdf.]
Jolliffe, I. T., and D. B. Stephenson (2003), *Forecast Verification: A Practitioner's Guide in Atmospheric Science*, 240 pp., John Wiley, Chichester.
Lakshmanan, V., T. Smith, G. J. Stumpf, and K. Hondl (2007), The Warning Decision Support System–Integrated Information (WDSS-II), *Weather Forecasting*, *22*(3), 592–608.
Lensky, I. M., and D. Rosenfeld (2006), The time-space exchangeability of satellite retrieved relations between cloud top temperature and particle effective radius, *Atmos. Chem. Phys.*, *6*, 2887–2894.
Lima, M. A., and J. W. Wilson (2008), Convective storm initiation in a moist tropical environment, *Mon. Weather Rev.*, *136*, 1847–1864.
Manzato, A. (2005), The use of sounding derived indices for a neural network short-term thunderstorm forecast, *Weather Forecasting*, *20*, 896–917.
Manzato, A. (2007), A note on the maximum Peirce skill score, *Weather Forecasting*, *22*, 1148–1154.
Masters, T. (1995), *Neural, Novel and Hybrid Algorithms for Time Series Prediction*, 514 pp., John Wiley, New York.
Mecikalski, J. R., and K. M. Bedka (2006), Forecasting convective initiation by monitoring the evolution of moving cumulus in daytime GOES imagery, *Mon. Weather Rev.*, *134*, 49–89.
Mecikalski, J. R., W. M. MacKenzie, M. König, and S. Muller (2010a), Cloud-top properties of growing cumulus prior to convective initiation as measured by Meteosat Second Generation. Part 1. Infrared fields, *J. Appl. Meteorol. Climatol.*, *49*, 521–534.
Mecikalski, J. R., W. M. Mackenzie, M. Koenig, and S. Muller (2010b), Use of Meteosat Second Generation infrared data in 0–1 hour convective initiation nowcasting. Part 2. Use of visible reflectance, *J. Appl. Meteorol. Climatol.*, *49*, 2544–2558.
Mecikalski, J. R., P. Watts, and M. Koenig (2011), Use of Meteosat Second Generation Optimal Cloud Analysis fields for understanding physical attributes of growing cumulus clouds, *Atmos. Res.*, *102*, 175–190.
Mecikalski, J. R., P. Minnis, and R. Palikonda (2013), Use of satellite derived cloud properties to quantify growing cumulus beneath cirrus clouds, *Atmos. Res.*, *120–121*, 192–201.
Mecikalski, J. R., J. K. Williams, C. P. Jewett, D. Ahijevych, A. LeRoy, and J. R. Walker (2015), Optimizing use of geostationary satellite observations and the development of probabilistic 0–1 hour convective initiation nowcasts, *J. Climate Appl. Meteorol.*, *54*, 1039–1059.
Merk, D., and T. Zinner (2013), Detection of convective initiation using Meteosat SEVIRI: Implementation in and verification with the tracking and nowcasting algorithm Cb-TRAM, *Atmos. Meas. Tech.*, *6*, 1903–1918.

Mueller, C., T. Saxen, R. Roberts, J. Wilson, T. Betancourt, S. Dettling, N. Oien, and J. Yee (2003), NCAR Auto-Nowcast System, *Weather Forecasting*, *18*, 545–561.
Mueller, C. K., J. W. Wilson, and N. A. Crook (1993), The utility of sounding and mesonet data to nowcast thunderstorm initiation, *Weather Forecasting*, *8*, 132–146.
Nisi, L., P. Ambrosetti, and L. Clementi (2014), Nowcasting severe convection in the Alpine region: The COALITION approach, *Q. J. R. Meteorol. Soc.*, *140*, 1684–1699.
Pal, M. (2005), Random forest classifier for remote sensing classification, *Int. J. Remote Sens.*, *26*(1), 217–222.
Purdom, J. F. W. (1976), Some uses of high resolution GOES imagery in the mesoscale forecasting of convection and its behavior, *Mon. Weather Rev.*, *104*, 1474–1483.
Purdom, J. F. W. (1982), Subjective interpretations of geostationary satellite data for nowcasting, in *Nowcasting*, edited by K. Browning, pp. 149–166, Academic Press, New York.
Rasmussen, E. N., and D. O. Blanchard (1998), A baseline climatology of sounding-derived supercell and tornado forecast parameters, *Weather Forecasting*, *13*, 1148–1164.
Roberts, R. D., and S. Rutledge (2003), Nowcasting storm initiation and growth using GOES-8 and WSR-88D data, *Weather Forecasting*, *18*, 562–584.
Roberts, R. D., D. Burgess, and M. Meister (2006), Developing tools for nowcasting storm severity, *Weather Forecasting*, *21*, 540–558.
Roberts, R. D., A. R. S. Anderson, E. Nelson, B. G. Brown, J. W. Wilson, M. Pocernich, and T. Saxen (2012), Impacts of forecaster involvement on convective storm initiation and evolution nowcasting, *Weather Forecasting*, *27*, 1061–1089.
Rosenfeld, D., and G. Gutman (1994), Retrieving microphysical properties near the tops of potential rain clouds by multispectral analysis of AVHRR data, *Atmos. Res.*, *34*, 259–283.
Rosenfeld, D., and I. M. Lensky (1998), Satellite-based insights into precipitation formation processes in continental and maritime convective clouds, *Bull. Am. Meteorol. Soc.*, *79*, 2457–2476.
Rosenfeld, D., and W. L. Woodley (2000), Deep convective clouds with sustained supercooled liquid water down to −37.5°C, *Nature*, *405*, 440–442.
Rosenfeld, D., W. L. Woodley, T. W. Krauss, and V. Makitov (2006), Aircraft microphysical documentation from cloud base to anvils of hailstorm feeder clouds in Argentina, *J. Appl. Meteorol.*, *45*, 1261–1281.
Rosenfeld, D., W. L. Woodley, A. Lerner, G. Kelman, and D. T. Lindsey (2008a), Satellite detection of severe convective storms by their retrieved vertical profiles of cloud particle effective radius and thermodynamic phase, *J. Geophys. Res.*, *113*, D04208, doi:10.1029/2007JD008600.
Rosenfeld, D., J. H. Golden, and G. Kelman (2008b), Short-term forecasting of severe convective storms using quantitative multi-spectral satellite imagery—Phase 2. Final Report on SBIR Phase-2 Contract. 128 pp.
Ruzanski, E., V. Chandrasekar, and Y. Wang (2011), The CASA nowcasting system, *J. Atmos. Oceanic Technol.*, *28*, 640–655.
Strabala, K. I., S. A. Ackerman, and W. P. Menzel (1994), Cloud properties inferred from 8–12-μm data, *J. Appl. Meteorol.*, *33*, 212–229.
Swets, J. A. (1973), The relative operating characteristic in psychology, *Science*, *182*, 990–1000.
Wakimoto, R. M., and H. V. Murphey (2009), Analysis of a dryline during IHOP: Implications for convection initiation, *Mon. Weather Rev.*, *137*, 912–936.
Walker, J. R., W. M. MacKenzie, J. R. Mecikalski, and C. P. Jewett (2012), An enhanced geostationary satellite-based convective initiation algorithm for 0–2 hour nowcasting with object tracking, *J. Appl. Meteorol. Climatol.*, *51*, 1931–1949.
Walther, A., and A. Heidinger (2012), Implementation of the Daytime Cloud Optical and Microphysical Properties Algorithm in PATMOS-x, *J. Appl. Meteorol. Climatol.*, doi:10.1175/JAMC-D-11-0108.1, in press.
Walther, A., A. Heidinger, and W. Straka (2011), ABI algorithm theoretical basis document for DCOMP., version 2.0 NOAA/NESDIS, 61 pp.
Williams, J. K. (2014), Using random forests to diagnose aviation turbulence, *Mach. Learn.*, *95*(1), 51–70, doi:10.1007/s10994-013-5346-7.
Williams, J. K., D. Ahijevych, S. Dettling, and M. Steiner (2008), Combining observations and model data for short-term storm forecasting, in *Remote Sensing Applications for Aviation Weather Hazard Detection and Decision Support, SPIE Proc.*, vol. 7088, edited by W. Feltz and J. Murray, 708805 pp., Intl. Soc. for Opt. Eng., doi:10.1117/12.795737.
Wilson, J. W., and C. K. Mueller (1993), Nowcasts of thunderstorm initiation and evolution, *Weather Forecast.*, *8*, 113–131.
Wilson, J. W., and W. E. Schreiber (1986), Initiation of convective storms by radar-observed boundary layer convergent lines, *Mon. Weather Rev.*, *114*, 2516–2536.
Wilson, J. W., G. B. Foote, N. A. Crook, J. C. Fankhauser, C. G. Wade, J. D. Tuttle, C. K. Mueller, and S. K. Kruger (1992), The role of boundary–layer convergence zones and horizontal rolls in the initiation of thunderstorms. A case study, *Mon. Wea. Rev.*, *120*, 1785–1815.
Wilson, J. W., N. A. Crook, C. K. Mueller, J. Sun, and M. Dixon (1998), Nowcasting thunderstorms: A status report, *Bull. Am. Meteorol. Soc.*, *79*, 2079–2099.
Wilson, J. W., Y. Feng, M. Chen, and R. D. Roberts (2010), Nowcasting challenges during the Beijing Olympics: Successes, failures, and implications for future nowcasting systems, *Weather Forecasting*, *25*, 1691–1714.
Wolfson, M. M., and D. A. Clark (2006), Advanced aviation weather forecasts, *Lincoln Lab. J.*, *16*(1), 31.
Ziegler, C. L., E. N. Rasmussen, M. S. Buban, Y. P. Richardson, L. J. Miller, and R. M. Rabin (2007), The "Triple Point" on 24 May 2002 during IHOP. Part II: Ground–radar and in situ boundary layer analysis of cumulus development and convection initiation, *Mon. Weather Rev.*, *135*, 2443–2472.
Zinner, T., H. Mannstein, and A. Tafferner (2008), Cb-TRAM: Tracking and monitoring severe convection from onset over rapid development to mature phase using multi-channel Meteosat-8 SEVIRI data, *Meteorol. Atmos. Phys.*, *101*, 191–210, doi:10.1007/s00703-008-0290-y.